Research Square

Preprints are preliminary reports that have not undergone peer review.
They should not be considered conclusive, used to inform clinical practice,
or referenced by the media as validated information.

Analysis of the Influence of Evolving Faults on Detection and Location Using Travelling-Wave Methods through Hardware-in-the-Loop Testing to SEL-T401L IED

Milton Ernesto Barrios Aguilar

miltonbarriosaguilar@gmail.com

Itaipu Parquetec

Daniel Motter

State University of West Paraná

Paulo Thiago de Godoy

Itaipu Parquetec

Tales Gottlieb Jahn

Itaipu Parquetec

Research Article

Keywords: Real Time Digital Simulator, TW87 Differential Protection, Ultra-High-Speed Line Relay, Computational Modeling, Double-ended e single-ended traveling-wave-based method

Posted Date: March 9th, 2026

DOI: https://doi.org/10.21203/rs.3.rs-8979294/v1

License: This work is licensed under a Creative Commons Attribution 4.0 International License.
Read Full License

Additional Declarations: No competing interests reported.

Version of Record: A version of this preprint was published at Journal of Control, Automation and Electrical Systems on August 27th, 2026. See the published version at https://doi.org/10.1007/s40313-026-01320-7.

Analysis of the Influence of Evolving Faults on Detection and Location Using Travelling-Wave Methods through Hardware-in-the-Loop Testing to SEL-T401L IED

Milton Ernesto Barrios Aguilar[1,2*], Daniel Motter[1,2†], Paulo Thiago de Godoy[1†], Tales Gottlieb Jahn[1†]

[1]Energy Management Center - GE.DT, Itaipu Parquetec, Tancredo Neves Avenue, Foz do Iguaçu, 85867-900, Parana, Brazil.
[2]Center of Engineering and Exact Sciences, Western Paraná State University, Tancredo Neves Avenue, Foz do Iguaçu, 85867-900, Parana, Brazil.

*Corresponding author(s). E-mail(s): miltonbarriosaguilar@gmail.com;
Contributing authors: daniel.motter@unioeste.br;
paulo.godoy@itaipuparquetec.org.br; tales.jahn@itaipuparquetec.org.br;
†These authors contributed equally to this work.

Abstract

Traveling-wave-based (TW-based) protection devices for fault detection and location on transmission lines are becoming increasingly prevalent in modern power systems due to their superior accuracy and fast operating performance. This study investigates modern fault detection and location techniques based on TWs using a commercial Intelligent Electronic Device (IED). The research focuses on a specific type of contingency, namely evolving faults. During single-phase faults with a **0°** fault inception angle, the amplitude of the generated TWs can be minimal or even imperceptible, hindering their detection and the accurate localization of the fault point by TW-based methods. However, if the fault evolves into a three-phase short circuit, the TW protection algorithm may successfully detect and locate the fault. Therefore, the objective of this research is to analyze this specific fault condition and evaluate how TW-based protection methods respond. To conduct the study, two SEL-T401L IEDs were connected to opposite ends of a transmission line in the Paraguayan interconnected power system of 50Hz, modeled on the RTDS simulation platform. A total of 154 tests were performed,

varying both the fault location and the fault evolution time. The results show that the SEL-T401L may fail to detect or locate faults using traveling-wave-based principles when the fault evolution time exceeds 35% of the power-frequency cycle (i.e., 7 ms). However, when a three-phase short circuit occurs within the first 35% of the cycle, the relay performs fast and accurate fault detection and location, with localization errors on the order of only a few meters.

Keywords: Real Time Digital Simulator, TW87 Differential Protection, Ultra-High-Speed Line Relay, Computational Modeling, Double-ended e single-ended traveling-wave-based method

1 Introduction

Technological advancements in protection equipment for Power Systems have driven the development of modern and efficient methods for fault detection and location. Among these methods, the use of Traveling Waves (TWs) stands out as an approach based on the identification of electromagnetic transients caused by disturbances in the grid power Burrell and Bhattarai (2024); Prado et al (2024); Wilches-Bernal et al (2021); Elhaffar (2008).

However, the application of TW technology faces challenges in specific situations, such as single-line-to-ground faults occurring with a fault inception angle close to 0°. Under these conditions, the amplitude of the generated TW may be minimal or imperceptible, making their detection difficult Martins et al (2023); Wright and Christopoulos (1993).

Furthermore, there are scenarios in which a single-line-to-ground fault evolves into a three-phase-to-ground fault after a certain time, generating TW in the transmission line only after this evolution. This type of event, known as an "evolving fault" Jiao and Liao (2017); Kumar et al (2022).

Although several studies have investigated fault-location methods for evolving faults and others have focused on enhancing traveling-wave-based detection and location techniques.

The application of TW methods to the location of evolving faults remains largely unexplored in the existing literature. As reported in Zhang et al (2017), a fully satisfactory solution for identifying and locating evolving faults in transmission lines using traveling-wave (TW) methods has not yet been established. The authors propose an integrated approach based on two sequential faults leading to a phase transition, combining TW characteristics and transient energy features to perform faulted-phase selection in two stages: at fault inception and shortly before fault clearance. However, the validation was conducted exclusively through simulation studies, without implementation on real equipment.

In the specific literature on evolutionary fault localization, the work in Ponukumati et al (2024) proposes a cross-correlation-based method to identify and locate evolving faults in unbalanced distribution systems—defined as sequential faults leading to a phase transition—using monitored signals at any network point, with results indicating that its accuracy is unaffected by fault location, resistance, or fault inception angle.

Jiao and Liao (2018) presented a novel approach for estimating the location of evolving faults in transmission lines using sparse wide-area voltage measurements, without requiring terminal measurements or prior information regarding the fault type or phase transition. However, the method does not incorporate detection based on TW techniques.

In addition, there are studies such as those by Singh and Bisht (2025); Jiao and Liao (2017); Kumar et al (2022) that investigate evolving fault detection and location using methods based on integrated mechanism based on signal processing and soft computing, the discrete wavelet transform, sparse wide-area measurements, and the Stockwell transform, Wigner distribution function and alienation coefficient, respectively. However, none of these studies address TW-based approaches.

Traveling-wave theory and its application to high-speed protection have been widely investigated. The study in Wilches-Bernal et al (2021) reviews signal-processing techniques for extracting information from power-system disturbances, surveys TW-based protection methods for transmission and distribution systems in both AC and DC networks, and discusses simulation tools for protection design and implementation.

The work in Haohao et al (2024) proposes a TW-based fault-location method for long high-voltage cables that considers dispersion effects and analyzes sheath currents at grounding and cross-bonding points, applying empirical wavelet transform (EWT) and multi-resolution singular value decomposition (MRSVD) to improve first-peak detection and distance estimation accuracy, with simulation results validating its effectiveness without direct high-voltage measurements.

Several studies based on traveling-wave theory analyze the performance and potential enhancements of single- and double-ended fault detection and location methods. Some of these studies also compare them with other approaches, such as impedance-based methods Wang et al (2025); Burrell and Bhattarai (2024); Elkin et al (2024); Liu et al (2024b); Lopes et al (2020); Martins et al (2023); Prado et al (2024); Salge et al (2022). However, these studies do not address evolving fault scenarios.

The objective of this study is to evaluate the performance of fault detection and location using TW methods in evolving fault scenarios, which start as A–ground faults with a fault inception angle of 0° and, after a certain time, evolve into ABC–G faults.

The tests were carried out on the real Paraguayan electrical system through Hardware-in-the-Loop (HIL) simulations using the Real-Time Digital Simulator (RTDS) and connecting two SEL-T401L Intelligent Electronic Device (IED) to protect the transmission line located between the Itaipu and Villa Hayes substations.

Section 2 describes the research methodology adopted for the HIL tests, including the modeling power system and the HIL integration. The results of the HIL simulations for three-phase, single-phase, and evolving faults are elucidated and discussed in Section 3. Finally, the research conclusions are presented in Section 4.

2 Method applied in HIL tests for analysis and evaluation of TW in evolutionary faults

To investigate the behavior of TWs under evolving fault conditions, it was necessary to configure the laboratory test bench and develop the required setup.

First, the Paraguayan power system was modeled, and the SEL-T401L IEDs were connected to the RTDS in a HIL configuration, enabling the evaluation of TW-based and impedance-based fault-location methods using both one-terminal and two-terminal approaches.

In this setup, the TW87 differential protection was configured as the primary function, while the TD21 and TW32 elements were included as backup protection functions.

The following subsections provide a comprehensive description of the adopted methodology.

2.1 The Itaipu 50 Hz System: Substep Implementation

The electric power system modeled in the RSCAD FX software of the RTDS platform was the 50 Hz Paraguayan National Interconnected System (SIN-PY), which represents the dynamics of the Paraguayan power system along with equivalents for Argentina and Uruguay. The system topology is shown in Figure 1 and consists of 75 nodes, 4 synchronous machines, 28 transmission lines, 3 shunt compensation banks, 3 two-winding transformers, 5 three-winding autotransformers, and 12 ZIP-model electrical loads. For further details on this power system, refer to Pesente et al (2021).

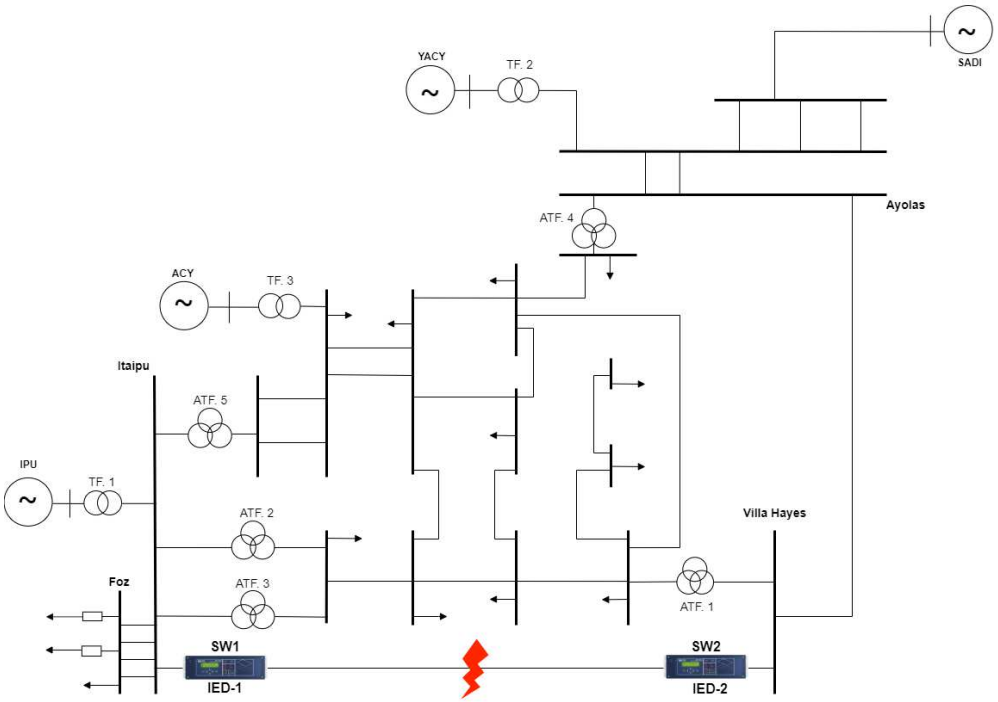


Fig. 1: Paraguayan National Interconnected System, used for testing Pesente et al (2021).

The 347 km Itaipu–Villa Hayes transmission line Pesente et al (2021) was selected for protection, with the IEDs installed at both ends. The Frequency-Dependent Phase (Fre-Phase) transmission line model was adopted, as it offers the highest accuracy for representing high-frequency traveling wave phenomena RTDS Tecnologies (2024).

In order to obtain higher-resolution results, the final step for accurate representation of TWs was to model this power system using substep simulation. This feature allows the grid power to be simulated with a significantly smaller time step than the main time step. Due to the capabilities of the RTDS available in the laboratory, the power system was divided into seven different substeps, resulting in a time resolution of 6666.67 ns.

Using RSCAD FX software, a fault control system was developed to simulate short-circuit events on the transmission line with different fault types, inception angles, evolution times and locations.

2.1.1 Connections for HIL Testing

HIL connections were established between the RTDS and the SEL-T401L IED, as shown in Figure 2. It should be noted that two identical IEDs were connected: one control circuit breaker SW1 (on the Itaipu bus, referred to as IED-1), and the other controls SW2 (on the Villa Hayes bus, referred to as IED-2); see Figure 2.

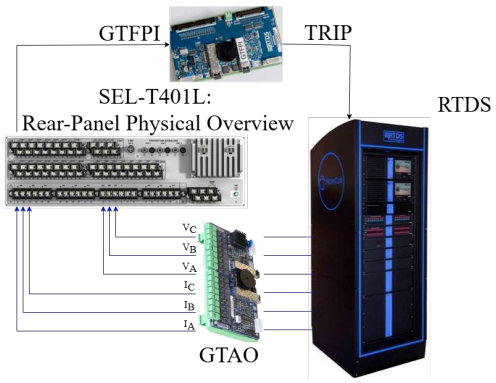


Fig. 2: HIL Connection: RTDS and SEL-T401L IEDs

As shown in Figure 2, the RTDS sends voltage and current signals to the IEDs through Giga-Transceiver Analogue Output (GTAO) Card, while the SEL-T401L relays send TRIP signals through Giga-Transceiver Front Panel Interface (GTFPI) Card to operate the simulated circuit breakers within the RTDS.

The SEL-T401L devices were configured to operate using the "TW87 Traveling-Wave Differential Protection", "TD21 Protection" and "TW32 Protection" schemes, as well as to perform fault location using single- and double-ended methods, based on both TW and impedance principles. The IED triggers the fault-location function immediately upon detection by any activated protection function.

2.2 Initial waves on lines when faults occur

TWs propagate in both directions from any point along a transmission line where voltage is abruptly disturbed by an event, such as a fault. Voltage TWs progressively modify voltage at other points on the line and are accompanied by current waves that redistribute charges on the line capacitance (Wright and Christopoulos, 1993).

The additional voltages and currents superimposed on the line during a conductor-to-conductor short-circuit can be determined by connecting a source at the fault location with an EMF equal in magnitude and opposite in polarity to that which would exist if the fault had not occurred (Wright and Christopoulos, 1993).

This situation is illustrated in Figure 3, from which it can be observed that the source EMF would be given by "e" if the voltage at the fault location F had been (Wright and Christopoulos, 1993):

$$V_f = V_{pf} * sin(\omega * t + \delta) \tag{1}$$

in the absence of the fault. In each case, the time t is measured from the time of the inception of the fault.

Analyzing Equation (1), it can be seen that if, at the initial instant of the fault ($t = 0$), the fault inception angle $\delta = 0^0$ or $\delta = 180^0$ does not propagate along the transmission line.

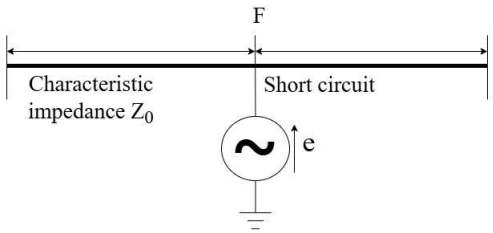


Fig. 3: Voltage and current waves on an A.C. line following a short-circuit (Wright and Christopoulos, 1993).

The initial value of the voltage TWs propagating away from the fault location (with fault resistance R_f between the conductors) is given by (Wright and Christopoulos, 1993):

$$V_1 = -\frac{Z_0}{Z_0 + 2 * R_f} * V_f \tag{2}$$

where Z_0 is the characteristic impedance of the line and V_f is the voltage given by Equation (1).

The initial values of the accompanying current waves, considering the wave directions as reference, are given by (Wright and Christopoulos, 1993):

$$I_1 = \frac{V_1}{Z_0} = \frac{1}{Z_0 + 2 * R_f} * V_f \tag{3}$$

It will be clear from equations (2) and (3) that the amplitudes of the TW reduce with increase of the resistance in the fault path. At the same time, it can be observed that V_1 and I_1 depend on V_f, that is, if the fault inception angle α is zero, then $V_1 = I_1 = 0$.

2.3 The SEL-T401L Intelligent Electronic Device and Fault Location Methods

This research implemented a HIL connection to the SEL-T401L IED. This high-performance line protection IED provides sampling rates in the microsecond range and TRIP times within the millisecond range. In addition, it includes line protection and fault location functions SEL (2022).

2.3.1 Fault Location Methods

Fault locators based on traveling waves provide highly accurate results within a tower span and offer significant benefits, including reduced outage time, lower repair costs, and prevention of fault recurrence Liu et al (2024a); SEL (2022); Tomasso et al (2019).

The fault-location function is initiated upon assertion of the IED TRIP bit. In its standard operating logic, the SEL-T401L activates the traveling-wave-based fault-location algorithm within 10 ms after trigger assertion when Port 6 is used, and within 60 ms when Ports 1, 2, or 3 are employed SEL (2022).

The methods used were the following:

- The double-ended traveling wave-based fault locator (DE-TWFL) operates on a simple principle, but requires communication between two IEDs and a common time reference.
  In the case applied in this research, the double-ended TW-based method operated using a fiber-optic channel that interconnected the two SEL-T401L IEDs.
  Figure 4 presents a Bewley diagram for a fault at location F on a line of length LL. The fault is located at a distance M (mi or km) from the local terminal (S) and at a distance LL-M (mi or km) from the remote terminal (R). The TW propagation velocity (VP) for the line is given by LL/TWLPT, where LL and TWLPT are the configured total line length and TW line propagation time, respectively.

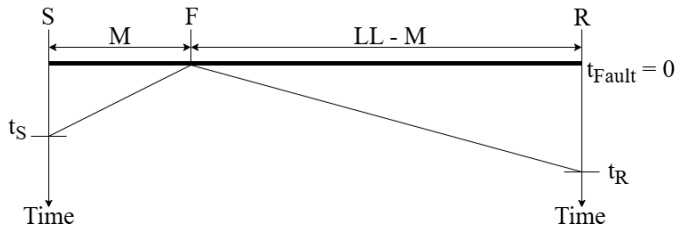


Fig. 4: Bewley diagram explaining double-ended TW based fault location method (SEL, 2022).

The first TW reaches the local terminal (S) at time t_S = M/VP. The first TW reaches the remote terminal (R) at time. The double-ended TW-based fault location method employs the following equation:

$$M = \frac{LL}{2}\left(1 + \frac{t_s - t_R}{TWLPT}\right) \tag{4}$$

- The single-ended traveling wave fault locator (SE-TWFL) eliminates the need for a communication channel and a common time reference; however, its operating principle is more complex. It is more cost-effective and less exposed to potential sources of error or failure. Figure 5 illustrates the Bewley diagram for the single-ended TW-based fault location method. The fault scenario is the same as in Figure 4, with the addition of a bus (B) located behind the local terminal (S), representing a bus connected to a line extending beyond terminal S.

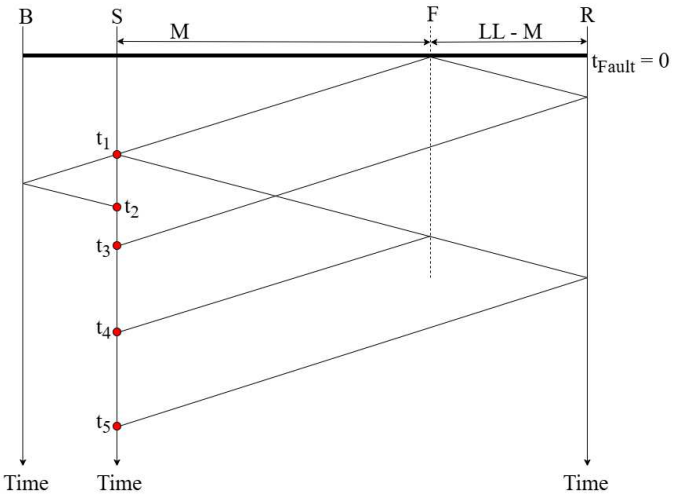


Fig. 5: Bewley diagram explaining single-ended TW based fault location method (SEL, 2022).

A current TW launched at the fault point (F) arrives at the local terminal (S) at time t_1. A portion of this wave is reflected, travels back to the fault point, reflects again, and then returns to the local terminal (S) at time t_4. During the time interval t_4 - t_1, the TW travels a distance of 2M.
Therefore, the single-ended TW-based fault location method applies the following equation:

$$M = \frac{(t_4 - t_1)}{2 * TWLPT} * LL \tag{5}$$

Due to the requirements of this investigation, fault location methods based on impedance were also investigated, as they are the most commonly applied in transmission lines.

These methods can be classified into single-ended and multi-ended approaches, depending on the number of terminals providing measurements Tomasso et al (2019). The used were the following:

- The double-ended impedance-based fault locator (DE-ZFL): uses voltages and currents from the local and remote terminals. As a consequence, it is necessary to have a communication channel and a common angle reference for the local and remote phasors. The double-ended impedance-based fault location method is founded on the principle of the negative-sequence voltage profile along the faulted transmission line. For balanced three-phase faults, the method instead utilizes the positive-sequence voltage profile.
  Figure 6 illustrates a negative-sequence voltage profile for a fault occurring at location F on a transmission line of length LL. The fault is located at a distance M (mi or km) from the local terminal (S) and at a distance LL-M (mi or km) from the remote terminal (R).

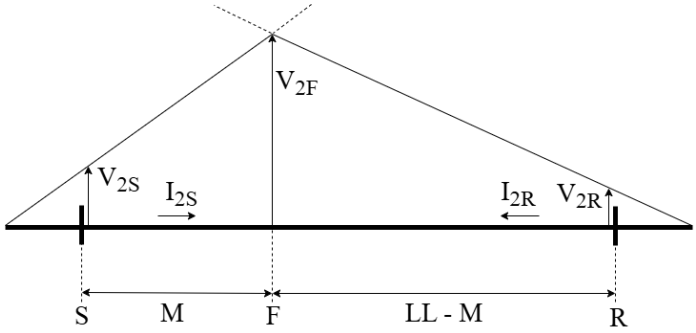


Fig. 6: Negative-Sequence Voltage Profile Explaining Double-Ended Impedance-Based Fault-Location Method (SEL, 2022).

The negative-sequence voltage at the fault location (V_{2F}), expressed in terms of the voltage and current at Terminal S, is given by:

$$V_{2F} = V_{2S} - \frac{M}{LL} * Z_1 * I_{2S} \tag{6}$$

The negative-sequence voltage at the fault location (V_2F), expressed in terms of the voltage and current at Terminal R, is given by:

$$V_{2F} = V_{2R} - \frac{LL - M}{LL} * Z_1 * I_{2R} \tag{7}$$

By comparing Equation (6) and Equation (7) and solving for M, the following equation is obtained:

$$M = LL * Re\left(\frac{V_{2S} - V_{2R} + Z_1 * I_{2R}}{Z_1 * (I_{2S} + I_{2R})}\right) \tag{8}$$

- The single-ended impedance-based fault locator (SE-ZFL): estimates the fault location using only local voltage and current measurements, together with the positive- and zero-sequence line impedance. The single-ended impedance-based fault location method uses negative-sequence current polarization for unbalanced faults and positive-sequence polarization for balanced three-phase faults.
  This method selects one of six protection measurement loops for further calculations based on fault type identification and utilizes local voltages and currents, as well as data from protection elements and schemes. For double-phase-to-ground faults, the method favors the phase loop over the two ground loops. For balanced three-phase faults, it uses positive-sequence voltages and currents.
  The polarization current I_{POL} is calculated as the negative-sequence current angle shifted to the selected loop. To locate the fault at point M (mi or km), the following equation is employed:

$$M = LL * \frac{Im\left(V_{LP} * I^*_{POL}\right)}{Im\left(Z_1 * I_{LP} * I^*_{POL}\right)} \tag{9}$$

For further details on the operation and accuracy of these four methods, consult Tomasso et al (2019); SEL (2022).

3 Results and Discussions: Three-Phase, Single-Phase, and Evolving Faults

3.1 Evaluation Method of Simulation Results

Initially, to observe the behavior of TWs and the IED response for three-phase and single-phase faults with a fault inception angle of 0°, seven initial HIL tests were conducted for each disturbance type, varying the fault location from 20% to 80% of the line length in 10% increments, taking the Itaipu bus as reference.

Subsequently, 140 evolving fault HIL tests were carried out. These simulations began with a single-phase A–G fault, with a 0° inception angle, which evolved into a three-phase ABC–G fault. The fault evolution was modeled across 20 time instants, ranging from 5% to 100% of the power frequency cycle in 5% increments, and for seven fault locations between 20% and 80% of the Itaipu line length, also in 10% increments.

The results were evaluated by analyzing the IED oscillographic records, focusing on the operation of the detection functions, the applied fault-location methods, and the corresponding accuracy. The location accuracy was assessed by computing the percentage error between the simulated fault point and the estimated one.

3.2 Types of simulated electrical faults and incidence angle

For all tests, electrical faults were simulated with a duration of 24 cycles, a fault resistance of 0.04Ω, and distances referenced from the Itaipu bus.

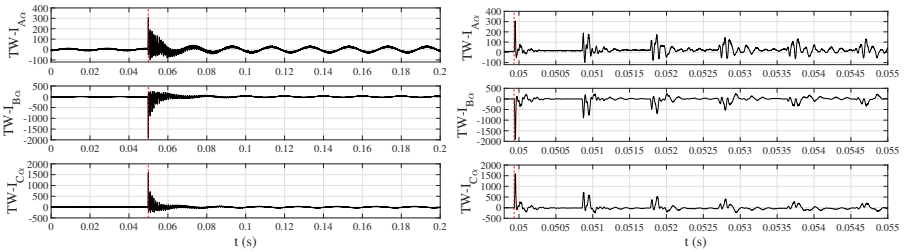
It should be noted that the presented cases and analyses refer to faults with a fault inception angle of 0°, with similar results observed for faults with an angle of 180°.

Furthermore, tests conducted with the RTDS indicate that the IEDs experience difficulties in detecting single-phase faults using TW methods when the inception angle is close to 0°, specifically within a range of ±3°.

3.3 Three-Phase-to-Ground Fault Test (ABC-G)

The first set of tests was performed for an ABC–G fault with a 0° fault inception angle, applied along the Itaipu–Villa Hayes transmission line at locations between 20% and 80% of the line length from the Itaipu bus, resulting in seven different test cases.

For illustrative purposes, Figure 7 shows the oscillographs, measured by IED-1, of alpha current TWs ($TW - I_\alpha$) for the specific case of a fault at 40% of the line (138.8 km from the Itaipu bus), along with the detail of the first $TW - I_\alpha$ (see Figure 7b).

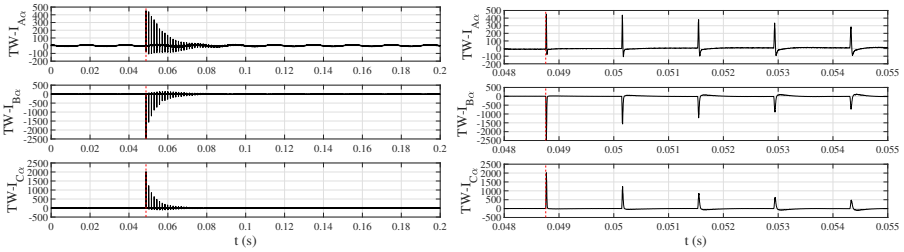


(a) TW Alphas, ABC-G Fault (b) Detail TW Alphas, ABC-G Fault

Fig. 7: Measurements at IED-1 During ABC-G Fault

It can be observed that the dashed red line indicates the fault inception, and that TWs are detected at the moment the fault occurs on the line.

Figure 8 presents the same test and the same electrical quantities as Figure 7; however, in this case, the measurements were taken by IED-2 installed at the Villa Hayes bus.



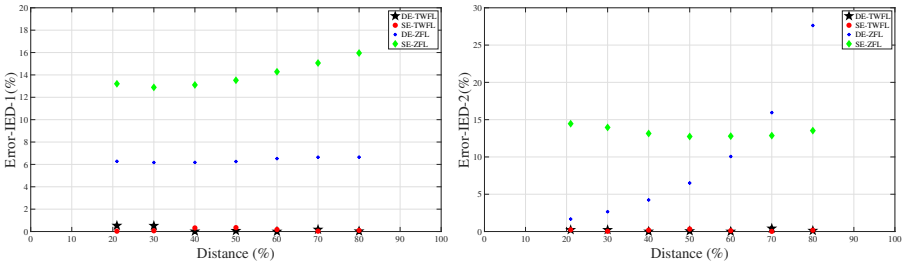
(a) TW Alphas, ABC-G Fault (b) Detail TW Alphas, ABC-G Fault

Fig. 8: Measurements at IED-2 During ABC-G Fault

The analysis of Figures 7 and 8, when evaluating the amplitude of the $TW - I_\alpha$, it was observed that phases B and C exhibit higher peaks, although TWs are also present in phase A. Furthermore, an appropriate reflection of the TWs measured by both IEDs was observed.

The considerations presented for this ABC-G three-phase fault case are analogous to those obtained for the seven three-phase faults evaluated. Furthermore, all TRIP signals issued by the IEDs in all ABC-G tests occurred in approximately 2 ms, through the TW87 protection.

Figure 9 shows the percentage errors obtained in each test. It can be observed that, for all fault locations, the IED detected the fault through TW and the fault location using both single- and double-ended methods achieved meter-level accuracy, with errors not exceeding 0.6%.



(a) Location error, ABC-G Fault, IED-1 (b) Location error, ABC-G Fault, IED-2

Fig. 9: Location error, ABC-G Fault

Although the fault location was detected using TW methods, the IEDs also performed calculations employing the impedance-based methods, and the location errors for these cases are shown in Figure 9.

It can be observed in Figure 9 that, with the single- and double-ended impedance methods, the location errors range approximately between 5% and 30%, meaning that the accuracy of these methods is on the order of kilometers.

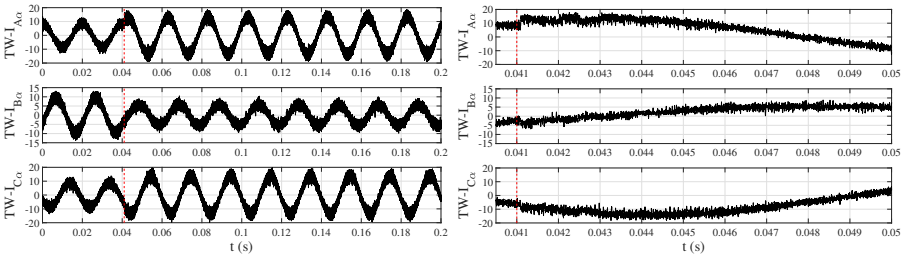
3.4 Single-Phase-to-Ground Fault Test (A-G)

The second set of tests, seven single-phase A-to-ground faults with a fault inception angle of 0° were simulated. Similar to the first set of test, the fault locations varied from 20% to 80% of the Itaipu-Villa Hayes line.

Figure 10 presents, for illustrative purposes, only the oscillographs for the fault case at 40% of the line, as the results for the other seven tests are identical. The dashed red line indicates the beginning of the fault period.

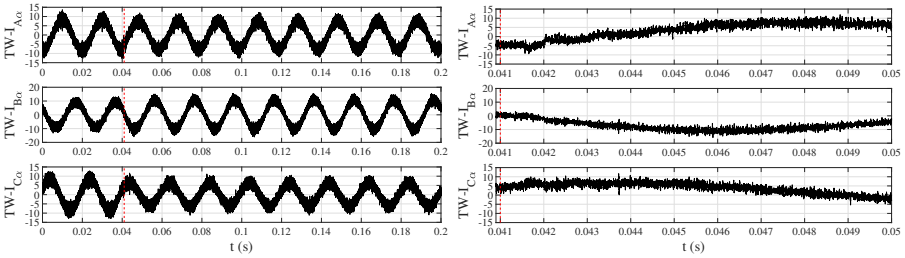
In the graphs of Figure 10, the alpha TWs measured by IED-1 can be observed.

In Figure 11, the $TW - I_\alpha$ measured by IED-2 are shown for the same single-phase fault case at 40% of the Itaipu line, along with the dashed red line indicating the beginning of the fault period.



(a) TW Alphas, A-G Fault (b) Detail TW Alphas, A-G Fault

Fig. 10: Measurements at IED1 During A-G Fault



(a) TW Alphas, A-G Fault (b) Detail TW Alphas, A-G Fault

Fig. 11: Measurements at IED2 During A-G Fault

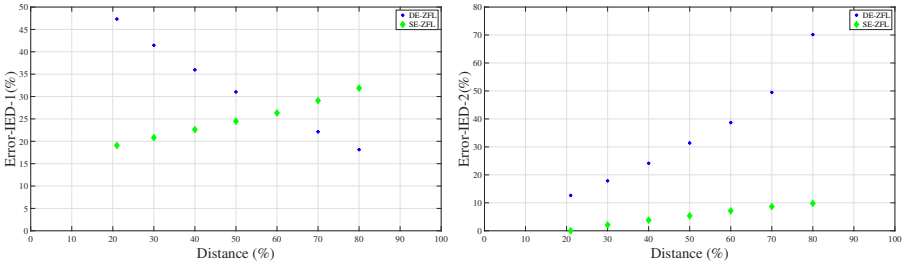
However, by examining Figures 10a, 10b, 11a and 11b, the absence of TWs during the A-to-ground fault tests with a fault inception angle of 0° can be observed, as predicted by Equation (1).

On the other hand, the IEDs detected the fault and issued the TRIP signal; however, due to the absence of TWs, the IEDs did not operate through TW87 or TW32 (they operated through the secondary TD21 function), with TRIP times on the order of 10 ms.

For these tests, due to the absence of TWs, the IEDs did not perform fault location using the TW methods (DE-TWFL or SE-TWFL). However, fault location using the impedance-based methods was carried out by the IEDs, and the errors are shown in Figure 12.

In these cases, the IEDs exhibited significant errors, on the order of kilometers.

Due to the fact that the IEDs cannot detect and locate faults using TW methods when single-phase faults occur with fault inception angles close to 0° or 180°, it is understood that secondary functions need to be implemented in the protection devices.



(a) Location error, AG Fault, IED1 (b) Location error, AG Fault, IED2

Fig. 12: Location error, AG Fault

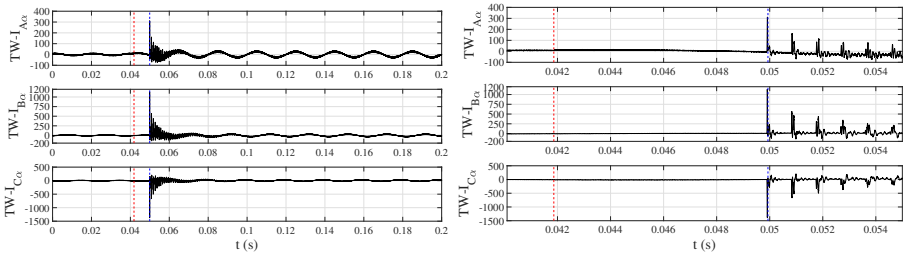
3.5 Evolving Fault Test: A-to-Ground to ABC-to-Ground

In this third set of test, 140 scenarios were simulated, all starting with a single-phase A-G fault with a 0° fault inception angle, which then evolved into a three-phase ABC-G fault. The evolution was carried out from 5% to 100% of the power-frequency cycle, in increments of 5% (totaling 20 different evolution times).

Furthermore, the tests were conducted for fault locations ranging from 20% to 80% of the Itaipu line length, in 10% increments, resulting in seven different distances.

An example case is shown in Figure 13 and 14, with the fault evolving at 50% of the power-frequency cycle and located at 40% of the line.

Similarly to the tests illustrated in Subsections 3.3 and 3.4, Figures 13 and 14 show the alpha current TWs measured by IED-1 and IED-2, respectively.

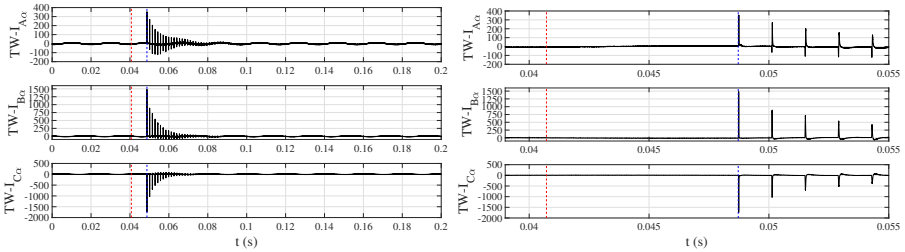


(a) TW Alphas, Evolving Fault (b) Detail TW Alphas, Evolving Fault

Fig. 13: Measurements at IED1 During A-G to ABC-G Fault

Furthermore, Figures 13 and 14 depict the fault evolution process, where the red dashed line represents the beginning of the A-G fault (with a 0° fault inception angle) and the blue dashed line represents the beginning of the ABC-G fault.

The evaluation of the TW ($TW - I_\alpha$) indicates that, although the current increases during the single-phase fault period, the TWs only appear when the fault becomes three-phase.



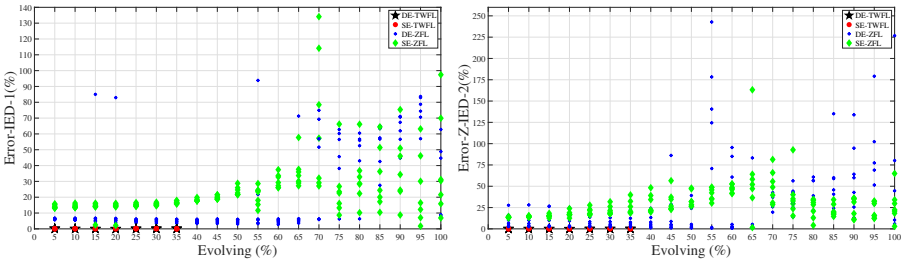
(a) TW Alphas, Evolving Fault (b) Detail TW Alphas, Evolving Fault

Fig. 14: Measurements at IED2 During A-G to ABC-G Fault

From that moment on, the behavior of the TWs remained similar to that observed in pure three-phase faults. In other words, the initial single-phase fault period did not influence the waveform, the maximum amplitudes, or the reflection times of the TWs during the three-phase fault.

As presented in the section 2.3.1 and due to the operation of the IED fault locator, for fault evolution times exceeding 7 ms, the IED disables the traveling-wave-based fault-location loop, and fault location is carried out solely by impedance-based methods.

Figure 15 presents the location errors calculated by the IEDs using TW methods. Due to the fault evolution process, the IEDs are able to estimate the location only up to 35% of the evolution cycle (7 ms). Thus, when the transition from A–G to ABC–G occurs after 7 ms, the IEDs are not longer able to determine the fault location using TW methods.



(a) Location error, Evolving Fault, IED1 (b) Location error, Evolving Fault, IED2

Fig. 15: Location error, AG to ABC-G Fault

At the same time, within the range in which the IEDs are able to estimate the fault location, the location errors are small, less than 0.6% and on the order of meters.

The analysis of the results obtained by the IEDs indicates that operation through TW87 differential protection is possible up to 85% cycle of fault evolution (17 ms). From 90% cycle (18 ms) onward, the relays operated through the TD21 distance element.

Figure 15 shows that, using impedance-based methods, the fault location estimate is independent of its evolution; however, the errors can be high, in some cases exceeding the total line length.

Regarding the operating time, when the SEL-T401L IEDs operate through the TW87 differential protection element, the TRIP signal is issued approximately 2 ms after the fault becomes three-phase. When the operation occurs through TD21, the TRIP occurs about 10 ms after the beginning of the single-phase fault period.

4 Conclusion

This paper presented Hardware-In-The-Loop tests involving the Paraguayan power system, modeled on the RTDS platform in substep, integrated with two SEL-T401L TW IEDs and protecting the Itaipu–Villa Hayes transmission line.

The study shows that the SEL-T401L accurately detects and locates three-phase-to-ground faults with a 0° inception angle, with errors below 0.6% when using TW87 and both SE-TWFL and DE-TWFL methods. For single-phase faults, TW information was insufficient, requiring backup protection (TD21) and impedance-based location methods.

For evolving faults, TW become observable only after the fault transitions to a three-phase condition, and their amplitude, reflection characteristics, and waveform shape are not affected by the duration of the initial single-phase fault period.

It is concluded that when the fault evolution time exceeds 7 ms, fault location is performed exclusively using impedance-based methods, as the IED no longer activates the traveling-wave-based fault-location loop.

In evolving faults, TWs became detectable only after the transition to a three-phase condition; accurate TW-based location was achieved for evolution times up to 35% of the cycle (7ms), while TW87 detection remained effective up to 85%.

Acknowledgments. The authors acknowledge the financial support of Itaipu Parquetec.

Declarations

Conflict of interest The authors declare that they have no conflict of interest.

References

Burrell J, Bhattarai P (2024) Novel approach to traveling-wave-based fault location in nonhomogeneous lines. In: 2024 IEEE Kansas Power and Energy Conference (KPEC). IEEE, pp 1–6, https://doi.org/10.1109/KPEC61529.2024.10676195, URL https://ieeexplore.ieee.org/document/10676195/

Elhaffar AM (2008) Power transmission line fault location based on current traveling waves. PhD thesis, Helsinki University of Technology

Elkin ST, Haider M, Roth TE (2024) Hybrid numerical modeling method for josephson traveling wave parametric amplifiers. In: 2024 IEEE International

Symposium on Antennas and Propagation and INC/USNC-URSI Radio Science Meeting (AP-S/INC-USNC-URSI). IEEE, pp 1979–1980, https://doi.org/10.1109/AP-S/INC-USNC-URSI52054.2024.10687127, URL https://ieeexplore.ieee.org/document/10687127/

Haohao C, Jing L, Ping C (2024) Design of fault location algorithm based on online distributed travelling wave for hv power cable. PLoS ONE 19. https://doi.org/10.1371/journal.pone.0296513

Jiao X, Liao Y (2017) An analytical approach to locate evolving faults on transmission lines based on sparse wide area measurements. In: 2017 IEEE Power and Energy Conference at Illinois (PECI). IEEE, pp 1–7, https://doi.org/10.1109/PECI.2017.7935721, URL http://ieeexplore.ieee.org/document/7935721/

Jiao X, Liao Y (2018) Accurate location of evolving faults on transmission lines using sparse wide area measurements. International Journal of Emerging Electric Power Systems 19. https://doi.org/10.1515/ijeeps-2017-0244

Kumar A, Sharma H, Mahia RN (2022) Evolving fault detection algorithm for transmission line protection. In: 2022 International Conference on Intelligent Controller and Computing for Smart Power, ICICCSP 2022. Institute of Electrical and Electronics Engineers Inc., https://doi.org/10.1109/ICICCSP53532.2022.9862408

Liu Q, Xu X, Chen Z, et al (2024a) Research on fault localization method of overhead line based on improved double-ended traveling wave method. 2024 4th International Conference on Energy, Power and Electrical Engineering (EPEE) pp 642–645. https://doi.org/10.1109/EPEE63731.2024.10875488, URL https://ieeexplore.ieee.org/document/10875488/

Liu S, Li W, Chen H, et al (2024b) Distribution network fault location configuration optimization method based on feature non-singular set. In: 2024 6th International Conference on Energy Systems and Electrical Power (ICESEP). IEEE, pp 986–989, https://doi.org/10.1109/ICESEP62218.2024.10651970, URL https://ieeexplore.ieee.org/document/10651970/

Lopes FV, Leite EJS, Ribeiro JPG, et al (2020) Phasor-based fault location challenges and solutions for transmission lines equipped with high-speed time-domain protective relays. Electric Power Systems Research 189. https://doi.org/10.1016/j.epsr.2020.106617

Martins JF, Martins A, Lopes R, et al (2023) Comparative analysis of travelling wave-based fault location method for different sampling. In: 2023 IEEE 17th International Conference on Compatibility, Power Electronics and Power Engineering (CPE-POWERENG). IEEE, pp 1–6, https://doi.org/10.1109/CPE-POWERENG58103.2023.10227433, URL https://ieeexplore.ieee.org/document/10227433/

Pesente J, Galassi P, Rodrigues L, et al (2021) A dynamic equivalent model for testing the paraguayan-argentinean interconnected power system devices using hardware-in-the-loop simulation. 2021 IEEE URUCON, URUCON 2021 pp 395–400. https://doi.org/10.1109/URUCON53396.2021.9647113

Ponukumati BK, Sinha P, Paul K, et al (2024) Evolving fault diagnosis scheme for unbalanced distribution network using fast normalized cross-correlation technique. PLOS ONE 19:e0305407. https://doi.org/10.1371/journal.pone.0305407, URL https://dx.plos.org/10.1371/journal.pone.0305407

Prado IF, Costa FB, Silva KM, et al (2024) High-frequency-based transmission line percentage differential protection with traveling wave alignment. IEEE Access pp 1–1. https://doi.org/10.1109/access.2024.3456040

RTDS Tecnologies (2024) RTDS - substep manual. Tech. rep., RTDS Tecnologies

Salge GS, Martins CM, Pereira PS, et al (2022) Realistic methodology for fault location and protection tests based on traveling waves. 16th International Conference on Developments in Power System Protection (DPSP 2022) pp 1–6. https://doi.org/10.1049/icp.2022.0948

SEL SEL (2022) SEL-T401L Ultra-High-Speed Line Relay Instruction Manual. Tech. rep., Schweitzer Engineering Laboratories

Singh SK, Bisht VS (2025) Soft computing based approach for ascertaining evolving faults in compensated lines. In: 2025 International Conference in Advances in Power, Signal, and Information Technology (APSIT). IEEE, pp 1–5, https://doi.org/10.1109/APSIT63993.2025.11086113, URL https://ieeexplore.ieee.org/document/11086113/

Tomasso AD, Invernizzi G, Vielmini G (2019) Accurate single-end and double-end fault location by traveling waves: a review with some real applications. In: 2019 AEIT International Annual Conference (AEIT). IEEE, pp 1–6, https://doi.org/10.23919/AEIT.2019.8893383, URL https://ieeexplore.ieee.org/document/8893383/

Wang Z, Liu S, Dragotti PL (2025) Faulted line identification in power distribution systems using convolutional neural networks and natural frequencies of travelling waves. IET Conference Proceedings 2025:121–126. https://doi.org/10.1049/icp.2025.0456, URL http://digital-library.theiet.org/doi/10.1049/icp.2025.0456

Wilches-Bernal F, Bidram A, Reno MJ, et al (2021) A survey of traveling wave protection schemes in electric power systems. IEEE Access 9:72949–72969. https://doi.org/10.1109/ACCESS.2021.3080234

Wright A, Christopoulos C (1993) Electrical Power System Protection. Springer US, https://doi.org/10.1007/978-1-4615-3072-5, URL http://link.springer.com/10.1007/978-1-4615-3072-5

Zhang G, Shu H, Liao Y (2017) An approach for detecting and locating evolving faults on transmission lines based on transient traveling waves. Electric Power Components and Systems 45:121–130. https://doi.org/10.1080/15325008.2016.1247390